2024 European Control Conference (ECC)
June 25-28, 2024. Stockholm, Sweden

On the optimal flywheel operation for inertial reaction mass wave energy conversion systems

Nicolás Faedo[a], Fabio Carapellese[a] and Bruno Paduano[a]

***Abstract*— This paper presents a direct transcription framework for optimising the operation of gyroscope-based inertial wave energy harvesters (WEH). In contrast to currently adopted procedures, we introduce a tailored optimal map as part of the total flywheel speed of the WEH, designed to maximise energy absorption. Since the target optimisation problem is infinite-dimensional, we derive a direct transcription process accordingly, exploiting tools from the field of *moment-based* theory. Following a formal derivation, the proposed framework is applied to a gyropendulum-based system, offering a numerical appraisal of the main characteristics underlying the methodology. We show that the procedure offered within this study is able to significantly enhance power absorption, hence contributing towards optimal energy-maximising operation of this family of systems.**

I. Introduction

The energy available in ocean waves has a massive potential towards effective decarbonisation, with estimates of available energy of up to 30,000 TWh/year [1]. As a matter of fact, recent efforts in exploitation of this resource have shown that wave energy harvesters (WEH), often also referred to as blue energy harvesters, are expected to replace traditional batteries in offshore applications [2]. These devices have the potential to play a significant role in meeting the growing global demand for clean and sustainable energy, and are expected to be exploited in a wide range of applications, including desalination and water treatment systems, as well as powering autonomous underwater vehicles, and sensor platforms used for ocean monitoring and data collection (see *e.g.* [3], [4]).

Internal reaction mass (IRM) WEH use the mechanical interaction between a floater and a rigid body to generate internal reaction forces, which can be of a different nature, *e.g.* inertial or elastic, having the advantage of a being fully enclosed absorption systems. Standard IRM devices can be generally classified in pendulum-based (such as *e.g.* [8]–[10]) and gyroscopic-based (see for instance *e.g* [11], [12]) systems. A particularly novel wave absorption concept has been presented for large-scale energy conversion in [16], which introduces the so-called *swinging omnidirectional wave energy converter*, referred to as SWINGO. This system is composed of a floating hull enclosing a *gyropendulum* device, combining pendulum and gyroscopic effects, exploiting both functionalities to activate an electromagnetic conversion system. An optimal operation of the gyropendulum is, naturally, fundamental to achieve reliable and efficient wave energy absorption, and enhance the operational performance of the overall WEH, hence unleashing its maximum potential.

Motivated by this, we present, in this paper, an optimisation framework for the optimal operation of the flywheel speed of a small-scale SWINGO device, adopted as a representative benchmark study for the family of IRM harvesting systems. In particular, in contrast to the state-of-the-art, which operates using a constant (and hence suboptimal) flywheel velocity (see *e.g.* [11]), we propose to incorporate an optimal speed regime as a function of the input wave period, computed based on an associated optimisation problem, which is formulated in an infinite-dimensional space. In order to transcribe such a problem into a tractable finite-dimensional nonlinear program, we exploit tools from so-called *moment-based* theory [17], leveraging the steady-state properties of the WEH system under analysis. We show that moment-based methods, which have been recently applied with success for optimal control of wave energy systems in *e.g.* [18], [19], provide a tailored tool for the optimisation of the operation regime of IRM WEH systems, showing significant improvements with respect to the methodology currently adopted within the literature.

The reminder of this paper is organised as follows. Section I-A introduces the main notation used within this study, while Section II briefly recalls the fundamentals of modelling for IRM WEH systems. Section III is the core of this paper, providing a formal derivation of the proposed moment-based optimisation methodology. Finally, Section IV offers a numerical appraisal of the main characteristics of the proposed technique with application to the SWINGO system, while Section V encompasses the main conclusions of this paper.

A. Notation and conventions

$\mathbb{R}^+$ denotes the set of non-negative real numbers. $\mathbb{C}_{<0}$ denotes the set of complex numbers with negative real part. The span of the set $X = \{x_i\}_{i=1}^k \subset \mathscr{Z}$, where $\mathscr{Z}$ is a vector space over a field $\mathbb{F}$, is denoted as $\text{span}(X)$. If $\mathscr{Z}$ is finite-dimensional, its dimension is denoted by $\dim(\mathscr{Z})$. The symbol 0 stands for any zero element, dimensioned according to the context, while $\mathbb{I}_n$ denotes the identity in $\mathbb{C}^{n\times n}$. The spectrum of a matrix $A \in \mathbb{C}^{n\times n}$ is denoted as $\lambda(A)$. Given two functions f_1 and f_2 in $L^2(\Xi) = \{f : \Xi \to \mathbb{R} \mid \int_\Xi |f(\tau)|^2 d\tau < +\infty\}$, their standard inner-product operation is $\langle f_1, f_2\rangle_\Xi = \int_\Xi f_1 f_2 \, \mathrm{d}t$. The notation $e_j^n \in \mathbb{R}^n$ is used for a vector with zeros everywhere but its j-th entry, which is set to 1 (*e.g.* $e_1^3 = [1\,0\,0]^\mathsf{T}$).

[a]N. Faedo, F. Carapellese and B. Paduano are with the Marine Offshore Renewable Energy Lab, Department of Mechanical and Aerospace Engineering, Politecnico di Torino, Italy (nicolas.faedo@polito.it).

II. Modelling fundamentals

SWINGO, schematically depicted in Figure 1, consists of an axisymmetric floating hull containing a gyropendulum system linked to a corresponding power take-off (PTO) axis, commonly termed ϵ-axis, that converts the associated gyropendulum motion into electric energy. Throughout this paper, we consider that the hull is constrained to move in pitch (δ), being the primary degree-of-freedom (DoF) for wave energy absorption, due to the positioning of the gyropendulum axis [16].

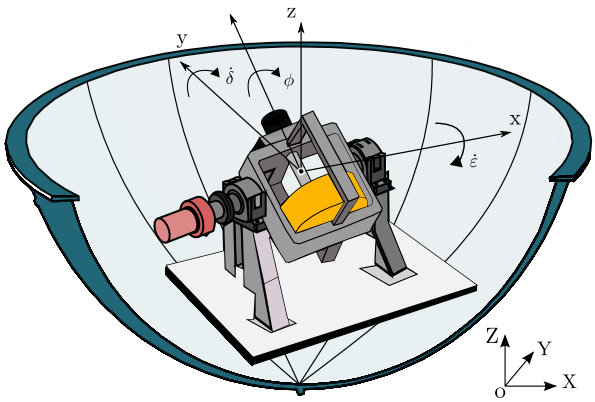

Fig. 1. Schematic illustration of the SWINGO system, including hull and gyropendulum mechanism.

The dynamics associated with SWINGO and, in general, any IRM WEH, can be modelled in terms of a set of differential equations, written as a continuous-time, finite-dimensional, dynamical system Σ, *i.e.*

$$\Sigma : \begin{cases} I_p\ddot{\delta} + H_{\mathrm{r}}\kappa + s_h\delta - J\phi\dot{\epsilon} = f_{\mathrm{e}}, \\ I_g\ddot{\epsilon} + k_{\mathrm{p}}\epsilon + J\phi\dot{\delta} - f_{\mathrm{PTO}}(\dot{\epsilon}) = 0, \\ \dot{\kappa} - F_{\mathrm{r}}\kappa - G_{\mathrm{r}}\dot{\delta} = 0, \end{cases} \tag{1}$$

where $\delta(t) \in \mathbb{R}$, denotes the (rotational) displacement in pitch, and $\epsilon(t) \in \mathbb{R}$ denotes the gyropendulum precession angle. The wave excitation torque, *i.e.* the external uncontrollable input due to the incoming wave field, is denoted by $f_{\mathrm{e}}(t) \in \mathbb{R}$. The state-vector $\kappa(t) \in \mathbb{R}^{n_{\mathrm{r}}}$, with $n_{\mathrm{r}} \in \mathbb{N}$, is used to denote the internal dynamics associated with radiation (memory dissipation) effects acting on the hull, fully characterised by the set of matrices $(F_{\mathrm{r}}, G_{\mathrm{r}}, H_{\mathrm{r}}^{\mathsf{T}}) \in \mathbb{R}^{n_{\mathrm{r}}\times n_{\mathrm{r}}} \times \mathbb{R}^{n_{\mathrm{r}}} \times \mathbb{R}^{n_{\mathrm{r}}}$. Note that $\lambda(F_{\mathrm{r}}) \subset \mathbb{C}_{<0}$ due to the passivity property associated with radiation effects (see [20]).

The parameter $s_h \in \mathbb{R}^+$ is the so-called hydrostatic stiffness, characterising hull restoring effects in pitch, while $k_{\mathrm{p}} \in \mathbb{R}^+$ is the gyropendulum mechanism stiffness. The set of parameters $\{I_p, J, I_g\} \subset \mathbb{R}^+$ denotes the inertia of the device in pitch (including the so-called added-inertia at infinite-frequency [6]), gyroscopic inertia, and total moment of inertia in the ϵ-axis, respectively. The PTO moment f_{PTO} is chosen here based upon a standard damping absorption law [21], *i.e.*

$$f_{\mathrm{PTO}}(t) = -b_{\mathrm{PTO}}\dot{\epsilon}(t), \tag{2}$$

with $b_{\mathrm{PTO}} \in \mathbb{R}^+$ designed according to the sea-state condition, based on the principle of maximum power transfer (see the discussion provided in Section IV-A). Note that, with this selection of f_{PTO}, the absorbed (mechanical) energy by the harvester, within an interval $\Xi = [0, T_w] \subset \mathbb{R}$, is given by

$$E(\dot{\epsilon}) = \frac{1}{T_w}\int_{\Xi} p(t)\mathrm{d}t = \frac{1}{T_w}\int_{\Xi} b_{\mathrm{PTO}}\dot{\epsilon}(t)^2\mathrm{d}t. \tag{3}$$

with $p(t) \in \mathbb{R}^+$ the instantaneous mechanical power.

Finally, the map $\phi : \mathbb{R}^+ \to \mathbb{R}$, $t \mapsto \phi(t)$, denotes the gyropendulum flywheel speed, which is the core concern of this paper. In particular, within the literature, $\phi(t)$ is always kept to a constant value $\phi^0 \in \mathbb{R}^+$, and hence not fully exploited to improve the performance of the harvester. In the light of this, within this study, we consider the map ϕ to be composed of a superposition of ϕ^0 and a user-defined zero-mean function $\psi \in L^2(\Xi)$, *i.e.*

$$\phi(t) = \phi^0 + \psi(t), \tag{4}$$

where ψ is to be optimised to maximise the mechanical energy absorption E in (3).

Aiming to provide a description of system Σ compatible with moment-based procedures (see Section III), we derive, in the following, a state-space representation of (1). Let $x = [\delta, \dot{\delta}, \epsilon, \dot{\epsilon}, \kappa^{\mathsf{T}}]^{\mathsf{T}}$, $x(t) \in \mathbb{R}^n$, with $n = 4 + n_{\mathrm{r}}$, be the state-vector associated with the SWINGO system. Define

$$A^0 = \begin{bmatrix} 0 & 1 & 0 & 0 \\ -\frac{s_h}{I_p} & 0 & 0 & \frac{J\phi^0}{I_p} \\ 0 & 0 & 0 & 1 \\ 0 & -\frac{J\phi^0}{I_g} & -\frac{k_{\mathrm{p}}}{I_g} & -\frac{b_{\mathrm{PTO}}}{I_g} \end{bmatrix}, \; B^0 = \begin{bmatrix} 0 \\ \frac{1}{I_p} \\ 0 \\ 0 \end{bmatrix}, \tag{5}$$

$$g_\psi(x,\psi) = \begin{bmatrix} 0 \\ \frac{J\psi}{I_p}x_4 \\ 0 \\ -\frac{J\psi}{I_g}x_2 \end{bmatrix}.$$

Exploiting the definitions provided in (5), a state-space representation for system Σ can be readily written as

$$\Sigma : \{\dot{x} = f(x,\psi,f_{\mathrm{e}}) = Ax + Bf_{\mathrm{e}} + g(x,\psi), \tag{6}$$

where the pair of matrices $(A, B) \in \mathbb{R}^{n\times n} \times \mathbb{R}^n$, and mapping $g \in \mathcal{C}^\infty$, are given by the expressions below:

$$A = \begin{bmatrix} A^0 & -B^0H_{\mathrm{r}} \\ G_{\mathrm{r}}e_2^4 & F_{\mathrm{r}} \end{bmatrix}, \; B = \begin{bmatrix} B^0 \\ 0 \end{bmatrix}, \; g(x,\psi) = \begin{bmatrix} g_\psi(x,\psi) \\ 0 \end{bmatrix}. \tag{7}$$

Remark 1. Note that the map g in (7) is such that $g(0,0) = 0$ and $\partial g(0,0)/\partial x = 0$.

Remark 2 (Local stability). Via Remark 1, it is straightforward to check that $(x,\psi,f_{\mathrm{e}}) = (0,0,0)$ is an equilibrium point for $\dot{x} = f(x,0,0)$. In fact, note that the Jacobian linearisation of Σ about the zero equilibrium is

$$\partial\Sigma : \{\dot{x} = Ax + Bf_{\mathrm{e}}, \tag{8}$$

where $\lambda(A) \subset \mathbb{C}_{<0}$ for any physically meaningful values for the parameters involved in the definition of the SWINGO system, and hence the zero equilibrium of (6) is locally exponentially stable in the Lyapunov sense.

III. Optimal flywheel operation via moment-based theory

Within this section, we derive a methodology to optimise the flywheel velocity ϕ in (4), via the proposed mapping ψ, exploiting so-called *moment-based* theory [19]. To achieve this objective, we begin by providing a formal definition of the optimisation problem (P) considered to compute ψ: For a given wave excitation torque f_{e}, and mean velocity ϕ^0 in (4), find a zero-mean mapping ψ^{opt} which optimises the absorbed energy for the WEH as defined in (3), *i.e.*

$$\begin{aligned}(P): \psi^{\mathrm{opt}} = \arg \max_{\psi \in L^2(\Xi)} & E(e_4^n x), \\ & \text{subject to:} \\ & \dot{x} = Ax + Bf_{\mathrm{e}} + g(x,\psi), \\ & \psi \in [-\psi_{\mathrm{lim}}, \psi_{\mathrm{lim}}] \subset \mathbb{R},\ \forall t \in \Xi,\end{aligned} \tag{9}$$

where the value ψ_{lim} denotes the maximum admissible variation for ψ. Note that problem (P) in (9) is, effectively, carried over an infinite-dimensional space, so an appropriate transcription process is required, in order to generate an associated finite-dimensional nonlinear program. This is performed, within this paper, employing tools from moment-based theory, and exploiting steady-state properties of the WEH under analysis.

In particular, following moment-based transcription [19], we begin by expressing the external (uncontrollable) input f_{e} in terms of an associated implicit form description, *i.e.* an autonomous continuous-time signal generator $\mathcal{G}$, defined as

$$\mathcal{G}: \begin{cases} \dot{\upsilon} = S\upsilon, \\ f_{\mathrm{e}} = L_{\mathrm{e}}\upsilon, \\ S = \begin{bmatrix} 0 & \omega_{\mathrm{e}} \\ -\omega_{\mathrm{e}} & 0 \end{bmatrix}, \\ \upsilon(0) = \upsilon_0, \end{cases} \tag{10}$$

where the triple of matrices $(S, L_{\mathrm{e}}^{\mathsf{T}}, \upsilon(0)) \in \mathbb{R}^{2\times 2} \times \mathbb{R}^2 \times \mathbb{R}^2$ is minimal. Note that minimality of $(S, L_{\mathrm{e}}^{\mathsf{T}}, \upsilon(0))$ implies observability of $(S, L_{\mathrm{e}}^{\mathsf{T}})$ and reachability (*i.e.* excitability [22]) of the pair $(S, \upsilon(0))$. The wave frequency ω_{e} is defined in terms of the associated wave period T_w, *i.e.* $\omega_{\mathrm{e}} = 2\pi/T_w$.

Remark 3. While 'regular', *i.e.* monochromatic, excitation inputs are considered within this paper, a polychromatic counterpart can be obtained straightforwardly, by changing the eigenstructure of the matrix S in (10) accordingly (see [19]).

Even though the input wave torque is considered to be monochromatic, the corresponding optimal flywheel operation map ψ is not, in general, a monochromatic function. In order to achieve a suitable representation of ψ in (4) in terms of an implicit form description, we define the so-called *extended* signal generator $\widetilde{G}$, which essentially incorporates $\mathcal{G}$ while 'extending' its definition (see Remark 4) to a suitable higher dimensional space, *i.e.*

$$\widetilde{\mathcal{G}}: \begin{cases} \dot{\Upsilon} = \widetilde{S}\Upsilon, \\ f_{\mathrm{e}} = \begin{bmatrix} L_{\mathrm{e}} & 0 \end{bmatrix} \Upsilon = \widetilde{L_{\mathrm{e}}}\Upsilon, \\ \psi = \widetilde{L_\psi}\Upsilon, \\ \widetilde{S} = S \oplus \left(\bigoplus_{k=2}^{\nu} \begin{bmatrix} 0 & k\omega_{\mathrm{e}} \\ -k\omega_{\mathrm{e}} & 0 \end{bmatrix} \right), \\ \widetilde{L_{\mathrm{e}}} = \begin{bmatrix} L_{\mathrm{e}} & 0 \end{bmatrix}, \\ \Upsilon(0) = \begin{bmatrix} \upsilon_0 & \Upsilon_0 \end{bmatrix}, \end{cases} \tag{11}$$

where the pair of matrices $(\widetilde{S}, \Upsilon(0)) \in \mathbb{R}^{q\times q} \times \mathbb{R}^q$ is excitable, and $q = 2(1+\nu)$.

Remark 4. System (11) is an extension of (10) in the following sense. Let $\mathscr{X} = \mathrm{span}(\{\upsilon_1, \upsilon_2\})$ and $\widetilde{\mathscr{X}} = \mathrm{span}(\{\Upsilon_i\}_{i=1}^q)$. It is straightforward to see that $\lambda(S) \subset \lambda(\widetilde{S})$ and, given the excitability condition on the pairs $(S, \upsilon(0))$ and $(\widetilde{S}, \Upsilon(0))$, $\mathscr{X} \subset \widetilde{\mathscr{X}} \subset L^2(\Xi)$ with $\dim(\mathscr{X}) = 2 < \dim(\widetilde{\mathscr{X}}) = q$. Furthermore,

$$\begin{aligned} \mathscr{X} &= \mathrm{span}(\{\cos(\omega_{\mathrm{e}}t), \sin(\omega_{\mathrm{e}}t)\}), \\ \widetilde{\mathscr{X}} &= \mathrm{span}(\{\cos(k\omega_{\mathrm{e}}t), \sin(k\omega_{\mathrm{e}}t)\}_{k=1}^{\nu}), \end{aligned} \tag{12}$$

so that $\widetilde{\mathcal{G}}$ 'extends' $\mathcal{G}$ by adding ν harmonic functions of the fundamental frequency ω_{e} to the state-space description associated with such a signal generator.

Remark 5. Note that f_{e}, originally written in terms of the implicit form (10), is defined in terms of $\widetilde{\mathcal{G}}$ by simply using a corresponding inclusion operator, *i.e.* the map $\mathbb{R}^2 \hookrightarrow \mathbb{R}^q : L_{\mathrm{e}} \mapsto \widetilde{L_{\mathrm{e}}} = [L_{\mathrm{e}}\ 0]$.

Given the nature of the extended signal generator $\widetilde{\mathcal{G}}$, which generates both bounded and T_w-periodic mappings f_{e} and ψ, and the local exponential stability properties of the zero-equilibrium of the VEH system Σ (see Remark 2), there exists [23] a unique locally defined mapping $\pi : \mathbb{R}^q \to \mathbb{R}^n$ which solves the partial differential equation

$$\frac{\partial \pi(\Upsilon)}{\partial \Upsilon}\widetilde{S}\Upsilon = f(\pi(\Upsilon), \widetilde{L_\psi}\Upsilon, \widetilde{L_{\mathrm{e}}}\Upsilon), \tag{13}$$

such that the steady-state response x_{ss} of system (6), for a given trajectory $\Upsilon(t)$ of the signal generator (11), is fully characterised in terms of π, *i.e.* $x_{\mathrm{ss}}(t) = \pi(\Upsilon(t))$.

Following [24], we propose a candidate approximate solution $\pi(\Upsilon) \approx \widetilde{\pi}(\Upsilon) = \Pi\Upsilon$ for equation (13), *i.e.* an approximation of π in terms of the q-dimensional space $\widetilde{\mathscr{X}}$ generated by $\widetilde{\mathcal{G}}$. The computation of Π, for a given trajectory $\Upsilon(t)$, can be performed following a Galearkin-like procedure, where an associated residual map $\mathscr{R}$ is defined:

$$\mathscr{R}: \Pi\widetilde{S}\Upsilon - A\Pi\Upsilon - B\widetilde{L_{\mathrm{e}}}\Upsilon - g(\Pi\Upsilon, \widetilde{L_\psi}\Upsilon), \tag{14}$$

and minimised accordingly by orthogonal projection onto the approximation space $\widetilde{\mathscr{X}}$, *i.e.*

$$\widetilde{\mathscr{R}}: \langle \mathscr{R}, \Upsilon^{\mathsf{T}} \rangle_{\Xi} = 0. \tag{15}$$

Via direct algebraic manipulation, (16) can be brought to a nonlinear set of algebraic equations in compact form, *i.e.*

$$\widetilde{\mathscr{R}}: \Pi\widetilde{S} - A\Pi - B\widetilde{L_{\mathrm{e}}} - \widetilde{g}(\Pi, \widetilde{L_\psi})\mathscr{P}^{-1} = 0, \tag{16}$$

where

$$\begin{aligned}\mathscr{P} &= \langle \Upsilon, \Upsilon^{\mathsf{T}} \rangle_{\Xi} \in \mathbb{R}^{q\times q},\\ \widetilde{g}(\Pi, \widetilde{L_\psi}) &= \langle g(\Pi\Upsilon, \widetilde{L_\psi}\Upsilon), \Upsilon^{\mathsf{T}} \rangle_{\Xi} \in \mathbb{R}^{n\times q},\end{aligned} \tag{17}$$

and $\lambda(\mathscr{P}) \not\ni 0$ due to the excitability of $(\widetilde{S}, \Upsilon(0))$ [22].

Remark 6. Existence of solutions for equation (17) is always guaranteed for a sufficiently large dimension q in (11). Furthermore, $\widetilde{\pi}(\Upsilon(t)) \to \pi(\Upsilon(t)) = x_{\text{ss}}(t)$ as $q \to \infty$ (see [24]), *i.e.* the quality of the approximation $\widetilde{\pi}$ can be directly controlled by the dimension of $\widetilde{\mathcal{G}}$.

Direct substitution of the candidate steady-state solution $x \mapsto x_{\text{ss}} = \widetilde{\pi}(\Upsilon)$ in the objective map (3) yields

$$\begin{aligned}E(e_4^n\widetilde{\pi}(\Upsilon)) &= \frac{b_{\text{PTO}}}{T_w}\int_{\Xi}(e_4^n\Pi\Upsilon)(e_4^n\Pi\Upsilon)^{\mathsf{T}}\mathrm{d}t\\ &= \frac{b_{\text{PTO}}}{T_w}(e_4^n\Pi)\left(\int_{\Xi}\Upsilon\Upsilon^{\mathsf{T}}\mathrm{d}t\right)(e_4^n\Pi)^{\mathsf{T}},\\ &= \frac{b_{\text{PTO}}}{2}(e_4^n\Pi)(e_4^n\Pi)^{\mathsf{T}},\end{aligned} \tag{18}$$

which is fully parameterised in terms of the solution Π associated with the set of equations (16).

Finally, by exploiting the moment-based equations (16) and (18), the infinite-dimensional optimisation problem (9) can be transcribed to a finite-dimensional nonlinear program, *i.e.*

$$\begin{aligned}\widetilde{(P)}: \psi^{\text{opt}} =& \widetilde{L}_\psi^{\text{opt}}\Upsilon,\\ \widetilde{L}_\psi^{\text{opt}} =& \arg\max_{\widetilde{L}_\psi^{\mathsf{T}}\in\mathbb{R}^q} \frac{b_{\text{PTO}}}{2}(e_4^n\Pi)(e_4^n\Pi)^{\mathsf{T}},\\ &\text{subject to:}\\ &\Pi\Upsilon - A\Pi - B\widetilde{L_{\text{e}}} - \widetilde{g}(\Pi, \widetilde{L_\psi})\mathscr{P}^{-1} = 0,\\ &\widetilde{L}_\psi\Upsilon \in [-\psi_{\text{lim}}, \psi_{\text{lim}}] \subset \mathbb{R},\ \forall t \in \mathcal{T}_\Xi,\end{aligned} \tag{19}$$

where the set $\mathcal{T}_\Xi = \{t_i\}_{i=1}^{\widetilde{N}} \subset \Xi$, with $\widetilde{N} > q$, $\widetilde{N} \in \mathbb{N}$, is a set of collocation points, uniformly distributed in Ξ, used to enforce the flywheel operational constraints in terms of the state-vector Υ. Note that, as expected from the transcription procedure, problem $\widetilde{(P)}$ in (19) is carried over the q-dimensional space $\mathbb{R}^q$, as opposed to problem (P) in (19), which is defined over $L^2(\Xi)$. Problem (19) can be solved using standard optimisation routines, *e.g.* sequential quadratic programming methods [25].

IV. Numerical Study

Within this section, we present a numerical appraisal of the application of the technique proposed in Section III. In particular, we consider a 1:s_f scale, with $s_f = 20$, SWINGO WEH system[1], as presented in Section II and conceptualised (in full scale) in [16]. We refer the reader to [16] for a full account on the computation of the parameters involved in (1). For the numerical analysis, regular waves are considered, with a fixed wave height of $2/s_f$ [m], and corresponding wave periods T_w in the set $[4/\sqrt{s_f},\ 8/\sqrt{s_f}]$ [s]. Note that the hydrodynamic resonance in pitch for this device is located at $T_r \approx 6.5/\sqrt{s_f}$ [s]. The mean (constant) velocity in (4) is set to $\phi^0 = 90$ [rad/s], while the limit value for the computation of ψ^{opt} in (19) is set to $\phi_{\text{lim}} = 0.5\phi^0$, *i.e.* ψ^{opt} can take values in $\pm 50\%$ of the mean velocity ϕ^0.

A. Tuning of b_{PTO}

The value for b_{PTO} in (2) needs to be tuned accordingly, to maximise energy absorption for each considered sea state. Within this paper, we follow the standard procedure used when $\phi = \phi^0$ in (4), *i.e.* $\psi = 0$ is considered. In this situation, tuning of b_{PTO} can be performed by exploiting the theory of maximum power transfer [26], since system (6) is effectively linear when $\psi = 0$ (see also Remark 2 and equation (8)). In particular, let $G : \mathbb{R} \to \mathbb{C}$,

$$G(\omega) = e_2^n(\jmath\omega\mathbb{I}_n - A)^{-1}B, \tag{20}$$

be the frequency response associated with the input-output map $f_{\text{e}} \mapsto \dot{\delta} = x_2$ in (8). Following maximum power transfer theory, the value of b_{PTO} is chosen in terms of the inverse map of (20), *i.e.*, for a given input frequency ω_{e}:

$$b_{\text{PTO}} = |G(\omega_{\text{e}})^{-1}|. \tag{21}$$

B. Optimal flywheel operation

We begin by presenting a numerical analysis on the selection of the dimension associated with the extended signal generator (11), *i.e.* the number of harmonics $q/2 = 1 + \nu$, and its influence on the optimality of the solution ψ^{opt}. Recall that this value defines the dimension of the finite-dimensional space over which problem $\widetilde{(P)}$ is effectively solved. In particular, Figure 2 shows the ratio between the absorbed energy for the WEH with an optimal velocity ψ^{opt} computed with a given number of harmonics $q/2$, termed $E^{q/2}$, and that computed with a sufficiently large number $q/2 = 20$, *i.e.* E^{20}. The latter has been chosen as a 'maximum' energy benchmark, since numerical experience shows virtually zero improvement for this WEH by adding more than 20 components to the signal generator (11). Based on Figure 2, a value of $q/2 = 10$ is adopted from now on, being this a reasonable compromise between optimality and computational complexity for solving problem (19), with an energy absorption of about 99% of E^{20}.

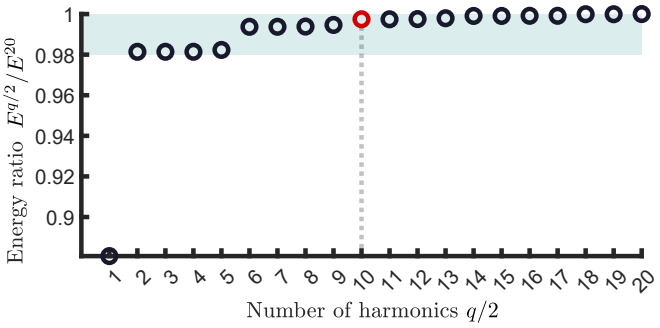

Fig. 2. Number of harmonics and its influence on the optimality of the solution.

[1]All quantities involved in this section are referred explicitly to their full scale counterparts, to facilitate a direct comparison with [16].

Having defined the dimension of the approximation space in $\widetilde{(P)}$, we analyse the performance improvement that can be achieved by the flywheel optimisation procedure proposed within this study. In particular, Figure 3 shows the ratio between the energy absorbed by considering the optimised flywheel velocity, *i.e.* $\psi = \psi^{\text{opt}}$ in equation (4), and by the 'baseline' benchmark methodology, *i.e.* $E = E_0$ with $\psi = 0$ in (4), for different wave periods.

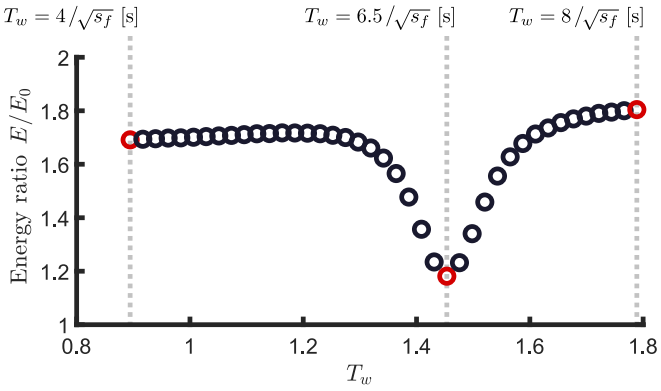

Fig. 3. Performance improvement achieved with the proposed moment-based optimisation.

The results presented in Figure 3 show that a significant performance improvement can be achieved by the proposed methodology, with up to $\approx 80\%$ more energy absorption, for both large and short wave periods. Note that, the smallest enhancement that can be achieved is, naturally, at the resonance period, where the designed f_{PTO} torque performs reasonably well in terms of energy absorption with a constant speed ϕ^0 (*i.e.* the baseline case). Nonetheless, even for this case, an enhancement in power absorption of $\approx 20\%$ can be appreciated, further demonstrating the capabilities of the proposed approach for the full operational bandwidth.

To illustrate the effect of the optimised flywheel operation in the overall WEH dynamics, Figure 4 presents a time-domain characterisation of the SWINGO system for three selected wave periods (marked in red within Figure 3). In particular, Figure 4 presents motion (first from the top), operational space (second from the top), instantaneous power (third from the top), and flywheel velocity (fourth from the top), for both baseline (solid-grey), and proposed moment-based (solid-black) methodologies. We begin by noting that, for all three cases, motion and operational space are enhanced by means of the proposed flywheel optimisation, taking larger values of velocity and position (especially for shorter and longer periods). This consistently translates, for the two extreme cases (left and right columns of Figure 4), in significantly larger instantaneous power values, producing a corresponding enhance in absorbed energy, as per Figure 3. It is interesting to note that, in resonance conditions (middle column of Figure 4), the optimised moment-based flywheel speed is capable of providing $\approx 20\%$ of energy absorption enhancement, while yet having smaller peak instantaneous power requirements than those exhibited by the baseline case. Finally, as can be appreciated in all three cases, we note that the optimised ψ^{opt} has a distinctive fundamental period, which corresponds to $T_w/2$. This is, naturally, not arbitrary, and can be traced back to the structure of the map g in (6): It is straightforward to show that, if ψ^{opt} has a fundamental period of $T_w/2$, the output of the map $g(x, \psi^{\text{opt}})$ (in steady-state) has a fundamental period of T_w due to the bilinearity of g, hence being able to generate a T_w-periodic contribution in Σ (*i.e.* coincident with the input wave), hence increasing the capabilities of ψ^{opt} to modify the VEH response.

V. Conclusions

This paper presents a tailored approach to optimise the flywheel operation regime for IRM WEH. In contrast to the standard procedure employed within the literature, a zero-mean map is introduced to the total flywheel speed of the WEH, designed to maximise energy absorption. Since the target optimisation problem is infinite-dimensional, a transcription process is derived accordingly, exploiting tools from the field of moment-based theory. Following a formal derivation, the proposed framework is applied to the SWINGO system, offering a numerical appraisal of the main characteristics of the methodology. In summary, it is shown that: The procedure proposed is able to significantly enhance power absorption, in the full operational bandwidth of the WEH system; and improvements of up to 80% can be obtained for the analysed WEH, for both short and long input wave periods. Overall, the proposed technique is able to enhance the performance associated with the IRM WEH in a wide set of operating conditions, hence contributing towards optimal energy-maximising operation of this family of systems. Future work will target an experimental analysis of this method for the SWINGO system, hence validating the proposed flywheel optimisation.

Acknowledgment

This project has received funding from the European Union's Horizon 2020 research and innovation programme under the Marie Sklodowska-Curie grant agreement No 101024372.

References

[1] G. Mork, S. Barstow, A. Kabuth, and M. T. Pontes, "Assessing the global wave energy potential," in *International Conference on Offshore Mechanics and Arctic Engineering*, vol. 49118, 2010, pp. 447–454.

[2] "Toward the blue energy dream by triboelectric nanogenerator networks," *Nano Energy*, vol. 39, pp. 9–23, 2017.

[3] M. Prauzek, J. Konecny, M. Borova, K. Janosova, J. Hlavica, and P. Musilek, "Energy harvesting sources, storage devices and system topologies for environmental wireless sensor networks: A review," *Sensors*, vol. 18, no. 8, p. 2446, 2018.

[4] T. Zhao, M. Xu, X. Xiao, Y. Ma, Z. Li, and Z. L. Wang, "Recent progress in blue energy harvesting for powering distributed sensors in ocean," *Nano Energy*, vol. 88, p. 106199, 2021.

[5] D. Ross, *Power From the Waves*. Oxford University Press, USA, 1995.

[6] J. Falnes and A. Kurniawan, *Ocean waves and oscillating systems: linear interactions including wave-energy extraction*. Cambridge university press, 2020, vol. 8.

[7] S. H. Salter, "Wave power," *Nature*, vol. 249, pp. 720–724, 1974.

[8] Y. Li, Q. Guo, M. Huang, X. Ma, Z. Chen, H. Liu, and L. Sun, "Study of an electromagnetic ocean wave energy harvester driven by an efficient swing body toward the self-powered ocean buoy application," *IEEE Access*, vol. 7, pp. 129 758–129 769, 2019.

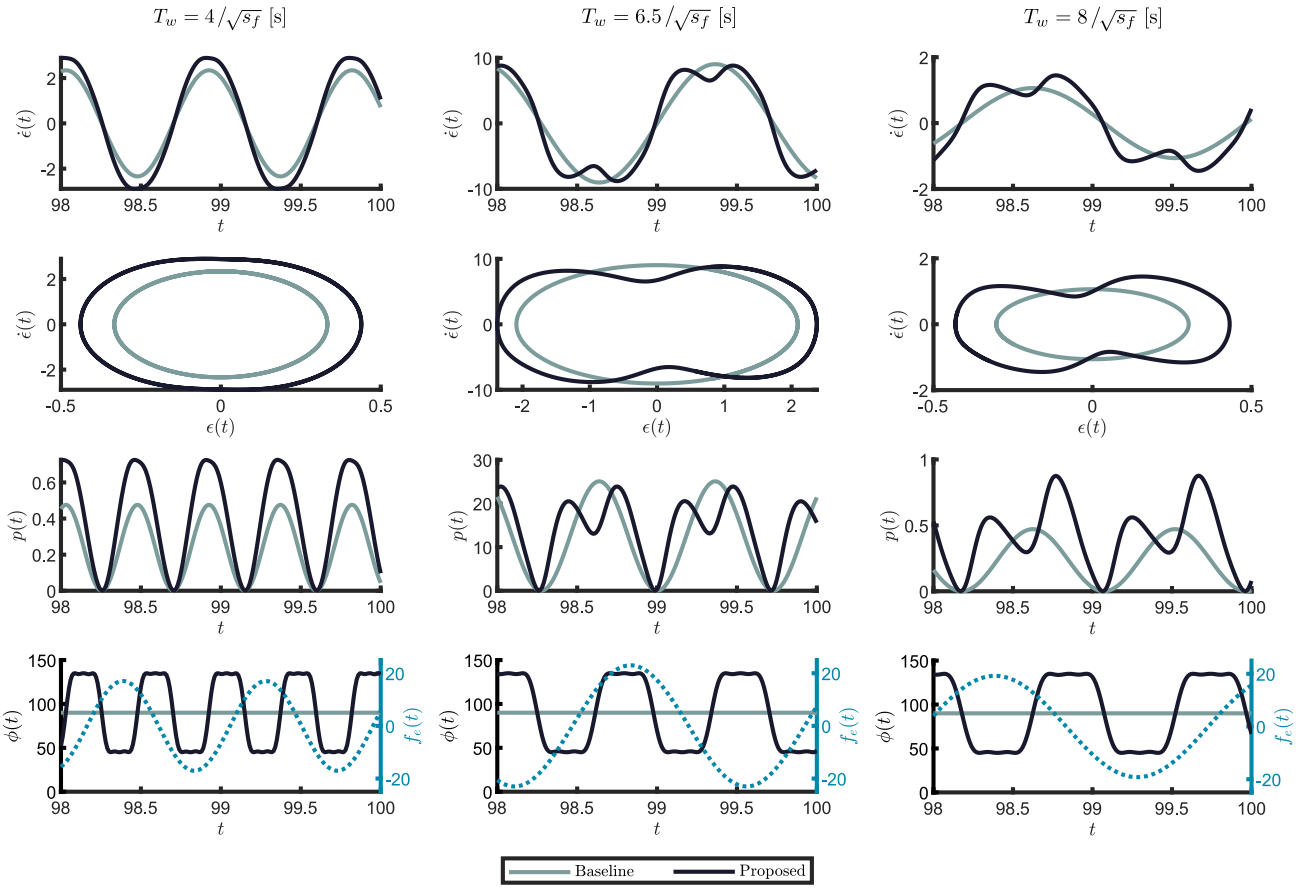

Fig. 4. Time-domain characterisation of the SWINGO system for three selected wave periods.

[9] N. Pozzi, G. Bracco, B. Passione, S. A. Sirigu, and G. Mattiazzo, "PeWEC: Experimental validation of wave to PTO numerical model," *Ocean Engineering*, vol. 167, pp. 114–129, 2018.

[10] W. Ding, H. Cao, B. Zhang, and K. Wang, "A low frequency tunable miniature inertial pendulum energy harvester," *Journal of Applied Physics*, vol. 124, no. 16, p. 164506, 2018.

[11] F. Carapellese, E. Pasta, N. Faedo, and G. Giorgi, "Dynamic analysis and performance assessment of the Inertial Sea Wave Energy Converter (ISWEC) device via harmonic balance," in *14th IFAC Conference on Control Applications in Marine Systems, Robotics and Vehicles*, Lyngby, Denmark, 2022.

[12] F. Salcedo, P. Ruiz-Minguela, R. Rodriguez Arias, P. Ricci, and M. Santos-Mujica, "Oceantec: Sea trials of a quarter scale prototype," in *Proceedings of 8th European Wave Tidal Energy Conference*, 2009.

[13] M. Previsic, A. Karthikeyan, and J. Scruggs, "A comparative study of model predictive control and optimal causal control for heaving point absorbers," *Journal of Marine Science and Engineering*, vol. 9, no. 8, p. 805, 2021.

[14] D. R. Herber and J. T. Allison, "Wave energy extraction maximization in irregular ocean waves using pseudospectral methods," in *International Design Engineering Technical Conferences and Computers and Information in Engineering Conference*, vol. 55881. American Society of Mechanical Engineers, 2013, p. V03AT03A018.

[15] R. Nie, J. Scruggs, A. Chertok, D. Clabby, M. Previsic, and A. Karthikeyan, "Optimal causal control of wave energy converters in stochastic waves–accommodating nonlinear dynamic and loss models," *Int. J. of Marine Energy*, vol. 15, pp. 41–55, 2016.

[16] F. Carapellese, E. Pasta, S. A. Sirigu, and N. Faedo, "SWINGO: Conceptualisation, modelling, and control of a swinging omnidirectional wave energy converter," *Mechanical Systems and Signal Processing (under review)*, 2023.

[17] A. Astolfi, G. Scarciotti, J. Simard, N. Faedo, and J. V. Ringwood, "Model reduction by moment matching: Beyond linearity a review of the last 10 years," in *2020 59th IEEE Conference on Decision and Control (CDC)*. IEEE, 2020, pp. 1–16.

[18] N. Faedo, G. Giorgi, J. Ringwood, and G. Mattiazzo, "Optimal control of wave energy systems considering nonlinear Froude–Krylov effects: control-oriented modelling and moment-based control," *Nonlinear Dynamics*, vol. 109, pp. 1777—1804, 2022.

[19] N. Faedo, G. Scarciotti, A. Astolfi, and J. V. Ringwood, "Nonlinear energy-maximizing optimal control of wave energy systems: A moment-based approach," *IEEE Transactions on Control Systems Technology*, vol. 29, no. 6, pp. 2533–2547, 2021.

[20] N. Faedo, Y. Peña-Sanchez, F. Carapellese, G. Mattiazzo, and J. V. Ringwood, "LMI-based passivation of LTI systems with application to marine structures," *IET Renewable Power Generation*, vol. 15, no. 14, pp. 3424–3433, 2021.

[21] N. Faedo, E. Pasta, F. Carapellese, V. Orlando, D. Pizzirusso, D. Basile, and S. A. Sirigu, "Energy-maximising experimental control synthesis via impedance-matching for a multi degree-of-freedom wave energy converter," *IFAC-PapersOnLine*, vol. 55, no. 31, pp. 345–350, 2022.

[22] A. Padoan, G. Scarciotti, and A. Astolfi, "A geometric characterization of the persistence of excitation condition for the solutions of autonomous systems," *IEEE Transactions on Automatic Control*, vol. 62, no. 11, pp. 5666–5677, 2017.

[23] A. Isidori, *Nonlinear Control Systems*. Springer, 1995.

[24] N. Faedo, G. Scarciotti, A. Astolfi, and J. V. Ringwood, "On the approximation of moments for nonlinear systems," *IEEE Transactions on Automatic Control*, vol. 66, no. 11, pp. 5538–5545, 2021.

[25] J. Nocedal and S. J. Wright, "Quadratic programming," *Numerical optimization*, pp. 448–492, 2006.

[26] N. Faedo, F. Carapellese, E. Pasta, and G. Mattiazzo, "On the principle of impedance-matching for underactuated wave energy harvesting systems," *Applied Ocean Research*, vol. 118, p. 102958, 2022.